Dynamic Modeling and Experimental Verification on the Rotor-Armature Structure of a Steam Turbine-Generator Unit

Hassan Jalali[a*], Farzad Rafieian[b], Hamed Haddad Khodaparast[c]

[a] Department of Mechanical and Construction Engineering, Northumbria University, Newcastle-upon-Tyne, NE1 8ST, United Kingdom

[b] Department of Mechanical Engineering, Arak University of Technology, Arak, 38181-41167, Iran

[c] College of Engineering, Swansea University, Bay Campus, Fabian Way, Crymlyn Burrows, Swansea, SA1 8EN, United Kingdom

Abstract

The rotor-armature structure of an exciter rotor used in a steam turbine-generator unit is investigated in this work. The objective is to create a base verified linear dynamic model of the exciter rotor for fault diagnosis or nonlinear interactions analysis. Natural frequencies for the rotor-armature structure are obtained from modal testing in free-free conditions. An analytical model for the structure is then constructed using Timoshenko beam theory, in which the linear effect of contact interface between rotor and armature is included. The unknown parameters of the rotor-armature model are identified by comparing analytical and experimental results. The verified dynamic model serves as the base for fault diagnosis and nonlinear response analysis due to the rotor and armature interactions.

Keywords: Rotor-armature; Structural modeling; Dynamic characteristic; Parameter identification.

[*] Corresponding author

1. Introduction

Dynamic modeling plays a crucial role in designing, analyzing, and predicting the response of structures. In rotating machinery, dynamic modeling also helps operation and maintenance procedures through fault diagnosis. Origins of malfunctions in a rotating machine reside in the rotor structure, stationary parts, or interactions of the two. These machines are assembled from thousands of parts, and thus, their measured vibratory response is a multitude of behavioral dynamics. The interference of dynamic effects complicates locating the specific signatures of the candidate faults for mitigation activities.

A dynamic model is employed to substantiate the behavioral characteristics of faults during operation. Such a tool serves the machine operators because there is no need to stop the machine for fault diagnosis unless necessary. A FE model of the rotor-bearing system for the exciter rotor of a 384 MW turbine generator unit is developed in [1] to diagnose its vibration problem. The model then recommends minor design changes and new alignments to remove the vibration problem. The effects of contact interfaces on torsional natural frequencies of a rod-fastened rotor used in heavy-duty gas turbines are studied in [2]. Contact elements incorporating torsional coefficients are defined between rotor segments fastened by long tie-bolts. It is shown that the annular contact surfaces have essential effects on the rotor stiffness and its dynamic characteristics. A 2D F.E. model of a gas turbine rotor considering the contact effects and pre-tightening forces of tie rods is developed in [3]. The model could reasonably predict the measured critical speeds of a real gas turbine rotor. In [4], an F.E. dynamic model of a disc-rotor for a gas turbine is developed. The study objectives in [4] were to investigate the effects of contacts between the discs and the rods' preload on the rotor natural vibration modes. The stiffness of contact elements for

the dynamic model of some rod-fastened rotors is identified in [5] using modal testing data. Tests are performed on laboratory samples, and the proposed method establishes a relationship between contact stiffness and contact stress. The method is then applied to a real gas turbine rotor. The influence of flexibly mounted bearings on the vibration response of a rigid gas turbine rotor is investigated in [6] using a 6DOF dynamic model. Conclusions are made based upon simulated responses for the optimum design of support characteristics that include a reduction in transmitted forces to the bearings by the synchronous response of unbalance rotor. Forced vibration analysis of mistuning and multistage coupling under rotation is performed using an F.E. model of the eight-stage shaft [7].

Dynamic models should be verified before being used for root cause analysis. For this purpose, an experiment with known inputs/outputs such as modal testing would serve the best. The output of modal tests - natural vibration modes - are the basic behavioral characteristics that a dynamic model should predict. To this aim, researchers employ innovative strategies to create accurate analytical / reduced-order, rather than detailed, F.E. models. The techniques usually provide modeling features for particular parts such as joints or frictional contact interfaces [8, 9] and use empirical parameters for tuning such as friction coefficients [10, 11]. This is especially important for structures such as rotor assemblies which contain contact interfaces [12-14], for which using detailed F.E. models become computationally expensive [15].

The effects of joints and contact interfaces on the dynamic response of rotors have been investigated by researchers in the past decade. Some literature surveys address rotor casing contact phenomena [16] and rotor to stator contacts in turbomachines [17]. The effect of blade-tip rubbing on the dynamic response of rotor systems has also been investigated inclusively [18, 19]. Nonlinear dynamics of a rotor system

containing a bolted flange joint are studied in [20]. It is shown by [21] through analytical modeling, including sticking and sliding phenomena for bolted joints of a rotor system that bolted joints produce stiffness loss and damping nonlinearity. The contact interface friction in the bolted joints of an aero-engine rotor system is considered in [22] to study the effect of friction coefficient on the dynamic behavior of the rotor. The effect of bolt loosening on the rotor dynamics was studied in [23]. They modeled the bending stiffness of the bolted disk-drum joint as a stepwise function of the relative rotation angle at the joint interface. Experimental and numerical methods are used in [24] to analyze the stiffness and contact state of joints and their effects on dynamic characteristics for aero-engine rotor systems. Time-varying stiffness caused by bolt loosening at rotating joint interface and its effects on rotor dynamics is studied in [23]. Calculation of contact stiffness for a rod-fastened rotor and its effects on rotor dynamics using an F.E. model is presented in [25]. Torsional effects are added to the rotor/stator contact model by [26], and the importance of its inclusion is highlighted through a numerical example with physical parameters. A new contact model for an assembled rotor-bearing system with several joints is proposed in [27] with a test set-up for validation. A method for modeling arbitrary geometries of contact with various surface roughness levels is proposed by [28] in rotor dynamic analysis. The test rig used in this study can impose various internal contact loads at different contact interface roughness levels to measure and study the system's natural frequencies. An empirical contact stiffness model for rotor assemblies is established in [29] and is validated by the authors in [30] on an actual tie bolt rotor designed for a high-pressure centrifugal compressor.

The rotor under study in this work is the exciter rotor of a 325 MW steam turbine-generator unit at Shazand Thermal Power Plant in Iran. The schematic in Figure 1 shows the rotor duty in operation. Records of measured vibrations by the CM

department on this rotor during the past few years have shown some abnormal behaviors, which raised concerns about its health condition. Therefore, during the overhaul period when the rotor was dismounted, the investigations reported in this article were carried out. A dynamic model was constructed for the rotor-armature structure. Modal tests in free-free boundary conditions are performed on the structure and its dynamic properties are extracted. An analytical model considering the effect of the contact between shaft and armature structures is developed using Timoshenko beam theory. The analytical model parameters are identified using the measured and simulated natural frequencies. It is worth mentioning that the core of this paper is about modeling, analysis, and identification of the rotor-armature structure. The numerical example considered in section 4 demonstrates the accuracy and applicability of the method presented in section 3. The novelty of this paper is twofold. First, A method is proposed based on the condition number of the coefficient matrix in analytical modeling, which offers advantages in finding natural frequencies. The second novelty of this research is applying the mathematical modeling and experimental updating strategies for a new field problem.

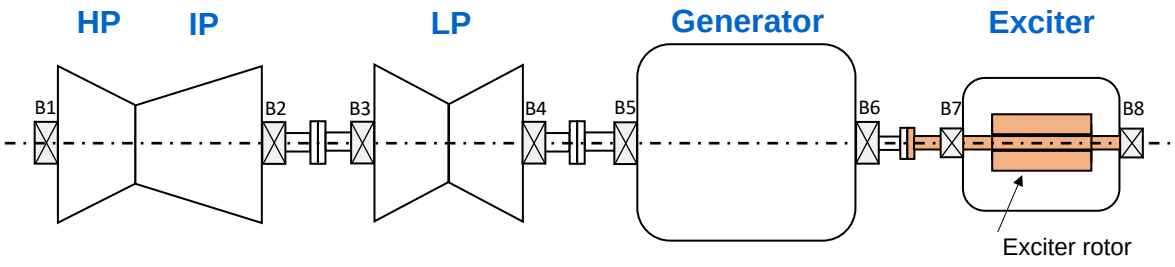

Figure 1: Schematic of the rotors chain in the 325 MW steam turbine-generator unit at Shazand Thermal Power Plant

The following section considers the experimental vibration analysis on the rotor-armature structure.

2. Experimental Vibration Analysis

The rotor-armature structure is shown in Figure 1, which consists of a shaft and an armature. The shaft is a stepped beam that is divided into 9 sections for the sake of convenience in modeling. The shaft is made of steel (i.e., $E_s = 210$ GPa and $\rho_s = 7800\ \mathrm{kg/m^3}$) has known dimensional and material properties. The length and diameter of different shaft sections are shown in Table 1. The rotor has a total length of $L = 3140$ mm.

The armature is made of copper coils inserted into armature slots. Therefore, in contrast to the shaft, the equivalent material properties of the armature are not known. One of the goals in this paper is to identify equivalent material properties for the armature. The armature has a total length of $L_{10} = 1361$ mm, an inner diameter of 220.4 mm, and an outer diameter of 625 mm. The connection between armature and shaft is a frictional contact type shown by green in Fig. 2. Another goal in this paper is to characterize the linear behavior of the contact interface by using experimental results.

Figure 2- the rotor-armature structure

Table 1- Length and diameter of different sections of the structure (mm)

Sec. No	1	2	3	4	5	6	7	8	9
Length	282	190	87.5	290	1361	532	112.5	190	95
Diameter	194	180	194	220.4	220.4	220.4	194	180	194

In experimental modal analysis, structures are tested in free-free conditions to minimize the effects of boundary conditions on the dynamic characteristics [31]. The free-free condition for rotor-armature structure is provided by suspending it using flexible belts, as shown in Fig. 3. The stiffness of the belts in the lateral direction is much lower than the flexural stiffness of the structure, and hence belts have a negligible effect on bending modes which are of the prime analysis concern in this paper.

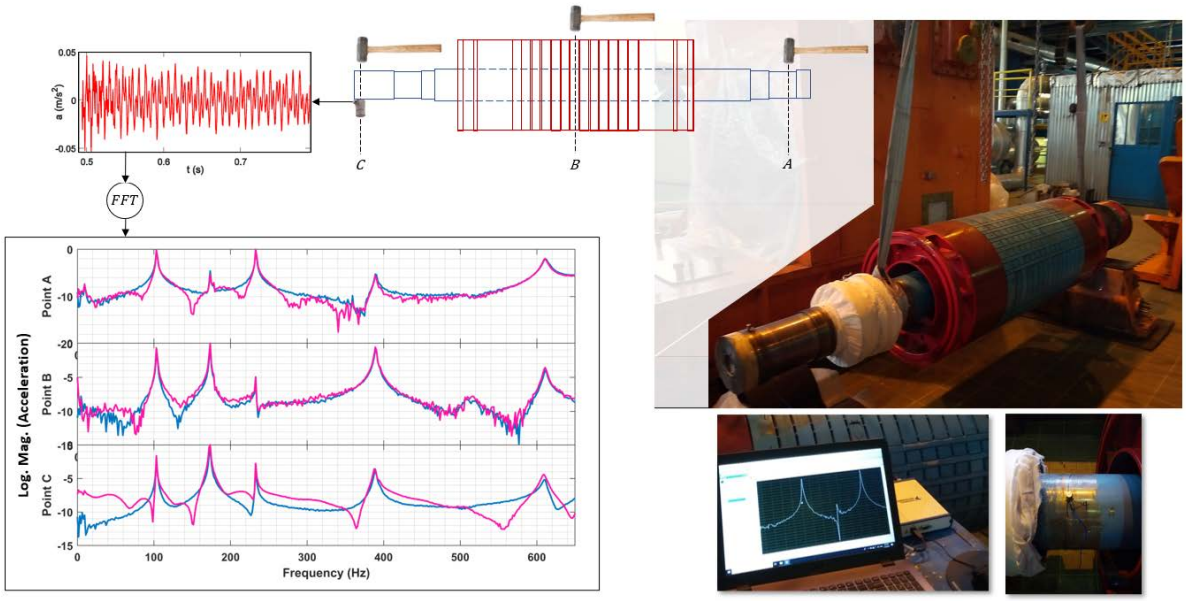

Figure 3. Experimental set-up and the experimental results

As stated earlier, the measurement of natural frequencies corresponding to bending modes is the foremost consideration in this paper. To this end, the structure is excited in the vertical direction in three points, i.e., points A, B and C, using a hammer

depicted in Fig. 3. For each excitation at one of these points, the free vibration response of the structure at points C is measured utilizing an accelerometer mounted at the end of the rotor. Since the free vibration response of structures contains natural frequencies, the measured signals in the time domain are transferred into the frequency domain by applying fast Fourier transform (FFT) to extract their frequency contents. Frequency contents of the measured signals representing the natural frequencies are reported in Table 2,

Table 2- measured natural frequencies of the rotor-armature structure (Hz)

ω_1	ω_2	ω_3	ω_4	ω_5
103.1	173.4	232.8	389.1	610.9

The measured natural frequencies are used in the following sections to construct an accurate model for rotor-armature structure. The following section considers mathematical modeling for the structure.

3. Mathematical Modelling

This section uses the Timoshenko beam theory to model the rotor-armature structure. A schematic of the mathematical model is depicted in Fig. 4, where different colors are used to show different sections of the structure. The normal and tangential stiffness effects of the contact interface between shaft and armature are considered by uniformly distributed continuous lateral and torsional springs with stiffness coefficients of k_w and k_t.

In total, the structure is divided into 10 sections (i.e., 9 sections on the shaft and 1 section on the armature) and section 5 on the shaft and section 10 on the armature are connected through lateral and torsional springs.

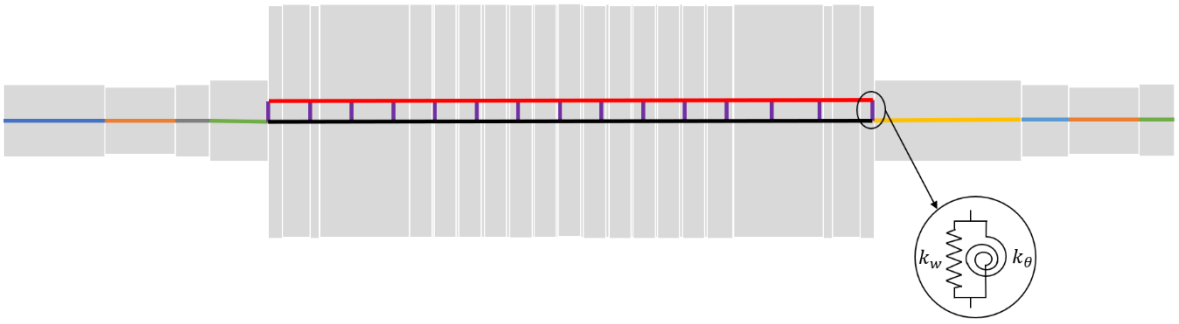

Figure 4- Schematic of the mathematical model

Using Timoshenko beam theory, governing equations for section i can be expressed as [32],

$$[M]_i \frac{\partial^2\{V(x,t)\}_i}{\partial t^2} + \Omega^2[G]_i \frac{\partial\{V(x,t)\}_i}{\partial t} + [E]_i \frac{\partial^2\{V(x,t)\}_i}{\partial x^2} + [D]_i \frac{\partial\{V(x,t)\}_i}{\partial t} + [K]_i\{V(x,t)\}_i + \{f(x,t)\}_i = 0, \quad i = 1,2,\dots,10 \tag{1}$$

where,

$$[M]_i = \begin{bmatrix} (\rho A)_i & 0 \\ 0 & (\rho I)_i \end{bmatrix},$$

$$[G]_i = \begin{bmatrix} 0 & 0 \\ 0 & -j(J_p)_i \end{bmatrix},$$

$$[E]_i = \begin{bmatrix} -(\kappa GA)_i & 0 \\ 0 & -(EI)_i \end{bmatrix},$$

$$[D]_i = \begin{bmatrix} 0 & (\kappa GA)_i \\ -(\kappa GA)_i & 0 \end{bmatrix},$$

$$[K]_i = \begin{bmatrix} 0 & 0 \\ 0 & (\kappa GA)_i \end{bmatrix}$$

$$\{V(x,t)\}_i = \begin{Bmatrix} w_i(x,t) \\ \psi_i(x,t) \end{Bmatrix}$$

$w_i(x,t)$ and $\psi_i(x,t)$ are deflection and angle of rotation of the cross-section due to bending moment for section i, respectively. A, I and J_p are respectively cross-

sectional area, cross-sectional moment of inertia and polar mass moment of inertia which are different for different structure sections. Ω is the shaft rotational speed. In the proceeding analyses, $\Omega = 0$ is used to comply with the experimental results used for model validation. ρ, E, G and κ are respectively density, Young's modulus, shear modulus, and shear constant. Shear modulus is related to Young's modulus by $G = E/2(1+\upsilon)$, and a Poison's ratio of $\upsilon = 0.3$ is used for both rotor and armature in this paper. Following equations are used for the shear constant of the shaft (solid circle) and armature (hollow circle) [33],

$$\kappa_r = \frac{6(1+\upsilon)}{7+6\upsilon},\ \kappa_a = \frac{6(1+\upsilon)(1+\chi^2)^2}{(7+6\upsilon)(1+\chi^2)^2+(20+12\upsilon)\chi^2} \tag{2}$$

where $\chi = R_i/R_o$ is the ratio of the inner radius to the outer radius of the armature.

It should be noted that ρ and E are the same for sections 1 to 9 and are equal to the material properties of steel since the rotor is made of steel. As stated before, equivalent material properties (i.e., density and modulus of elasticity) are unknown for the armature. They are identified by using experimental results in the next section. It is worth mentioning that in the following sections ρ_s and E_s are used as material properties for shaft and ρ_a and E_a as material properties for the armature. In equation (1), $\{f(x,t)\}_i = [f_{wi} \quad f_{ti}]^T$ contains the restoring forces in the lateral and torsional springs and are defined as

$$f_{wj}(x,t) = f_{tj}(x,t) = 0, \quad j = 1, \dots 4 \quad and \quad j = 6, \dots, 9 \tag{3}$$

$$f_{w5}(x,t) = -f_{w10}(x,t) = k_w(w_5(x,t) - w_{10}(x,t)) \tag{4}$$

$$f_{t5}(x,t) = -f_{t10}(x,t) = k_\theta\big(\psi_5(x,t) - \psi_{10}(x,t)\big) \tag{5}$$

Having the equation governing lateral vibration of different sections in equation (1), one may express equation governing the dynamic response of rotor-armature structure as,

$$[M]\frac{\partial^2\{V(x,t)\}}{\partial t^2}+[E]\frac{\partial^2\{V(x,t)\}}{\partial x^2}+[D]\frac{\partial\{V(x,t)\}}{\partial t}+[K]\{V(x,t)\}+\{F(x,t)\}=0 \quad (6)$$

where,

$$[M]=diag([[M]_1 \quad [M]_2 \quad \cdots \quad [M]_{10}])$$

$$[E]=diag([[E]_1 \quad [E]_2 \quad \cdots \quad [E]_{10}])$$

$$[D]=diag([[D]_1 \quad [D]_2 \quad \cdots \quad [D]_{10}])$$

$$[K]=diag([[K]_1 \quad [K]_2 \quad \cdots \quad [K]_{10}])$$

$$\{V(x,t)\}=[w_1(x,t) \quad \psi_1(x,t) \quad w_2(x,t) \quad \psi_2(x,t) \quad \ldots \quad w_{10}(x,t) \quad \psi_{10}(x,t)]^T$$

$$\{F(x,t)\}=[f_{w1}(x,t) \quad f_{t1}(x,t) \quad f_{w2}(x,t) \quad f_{t2}(x,t) \quad \ldots \quad f_{w10}(x,t) \quad f_{t10}(x,t)]^T$$

The following boundary conditions and compatibility requirements are applied to equation (6),

$$(EI)_1\frac{\partial\psi_1(x,t)}{\partial x}=(\kappa GA)_1\left(\frac{\partial w_1(x,t)}{\partial x}-\psi_1(x,t)\right)=0, \quad at \quad x=0 \quad (7)$$

$$(EI)_9\frac{\partial\psi_9(x,t)}{\partial x}=(\kappa GA)_9\left(\frac{\partial w_9(x,t)}{\partial x}-\psi_9(x,t)\right)=0, \quad at \quad x=L \quad (8)$$

$$(EI)_{10}\frac{\partial\psi_{10}(x,t)}{\partial x}=(\kappa GA)_{10}\left(\frac{\partial w_{10}(x,t)}{\partial x}-\psi_{10}(x,t)\right)=0, \quad at \quad x=L_1 \quad (9)$$

$$(EI)_{10}\frac{\partial\psi_{10}(x,t)}{\partial x}=(\kappa GA)_{10}\left(\frac{\partial w_{10}(x,t)}{\partial x}-\psi_{10}(x,t)\right)=0, \quad at \quad x=L_2 \quad (10)$$

$$w_s(x_s,t)=w_{s+1}(x_s,t),\ \psi_s(x_s,t)=\psi_{s+1}(x_s,t), \quad x_s=\sum_{r=1}^{s}L_r, \quad s=1,2,\ldots,8 \quad (11)$$

$$(EI)_s\frac{\partial\psi_s(x_s,t)}{\partial x}=(EI)_{s+1}\frac{\partial\psi_{s+1}(x_s,t)}{\partial x},\ x_s=\sum_{r=1}^{s}L_r, \quad s=1,2,\ldots,8 \quad (12)$$

$$(\kappa GA)_s\left(\frac{\partial w_s(x_s,t)}{\partial x}-\psi_s(x_s,t)\right)=(\kappa GA)_{s+1}\left(\frac{\partial w_{s+1}(x_s,t)}{\partial x}-\psi_{s+1}(x_s,t)\right),,\ x_s=\sum_{r=1}^{s}L_r, \quad s=1,2,\ldots,8 \quad (13)$$

Free vibration analysis of the rotor-armature structure is considered in this paper, which is performed by substituting $\{V(x,t)\}=\{Y(x)\}e^{j\omega t}$ in equations (6-13) resulting in the following equations,

$$[E]\frac{d^2\{Y(x)\}}{dx^2} + [D]\frac{d\{Y(x)\}}{dx} + [G]\{Y(x)\} = 0 \tag{14}$$

where $\{Y(x)\}$ contains functions defining the mode shapes corresponding to different sections of the structure and is defined as,

$$\{Y(x)\} = [W_1(x) \quad \Phi_1(x) \quad W_2(x) \quad \Phi_2(x) \quad \cdots \quad W_{10}(x) \quad \Phi_{10}(x)]^T \tag{15}$$

and $[G]$ is defined as,

$$[G] = [K] - \omega^2[M] + [F] \tag{16}$$

In equation (16), ω is the natural frequency and $[F]$ is given in Appendix. The equations governing boundary conditions and compatibility requirements subject to equation (14) are also given in Appendix.

Equation (14) defines a set of coupled second-order differential equations which can be solved by reducing them to a system of first-order differential equations of the form $\{\dot{z}\} = [H]\{z\}$, where

$$[H] = \begin{bmatrix} [0] & [I] \\ -[E]^{-1}[G] & -[E]^{-1}[D] \end{bmatrix}, \quad \{z\} = \begin{bmatrix} \{Y(x)\} \\ \frac{d\{Y(x)\}}{dx} \end{bmatrix} \tag{17}$$

Solving the above system of first-order differential equations results in,

$$\{z\} = \sum_{n=1}^{40} C_n\{b\}_n e^{\lambda_n x} \tag{18}$$

where C_n are constants and λ_n and $\{b\}_n$ are respectively eigenvalues and eigenvectors of $[H]$. Satisfying the boundary conditions and compatibility requirements defined in Appendix, a set of algebraic equations in terms of the constants $C_n, n = 1,2, \ldots ,40$ of the following form is obtained,

$$[Q(\omega, \rho_a, E_a, k_w, k_\theta)]\{c\} = 0 \tag{19}$$

where $\{c\} = [C_1 \quad C_2 \quad \dots \quad C_{40}]^T$ contains the constants, ω is the natural frequency, ρ_a and E_a are density and Younge's modulus of the armature and k_w and k_θ are equivalent linear stiffness coefficients of the contact interface between rotor and armature. $[Q]$ is a function of unknown parameters of the rotor-armature structural model.

Equation (19) can be used to find natural frequencies and mode shapes when all system parameters are known or identify the system parameters when some natural frequencies are known and some system parameters are unknown (i.e., similar to the case considered in this paper). In the former application of equation (19), where system parameters are all known, this equation reduces to $[Q(\omega)]\{c\} = 0$ and the natural frequencies are obtained by solving the characteristic equation, which is,

$$q(\omega) = |Q(\omega)| = 0 \tag{20}$$

where, $|o|$ denotes the determinant operator. Equation (20) is a polynomial that can be solved using numerical methods [34] and the natural frequencies ω_ns can be obtained. Having known the natural frequency ω_n from the characteristic equation solution, i.e. equation (20), one may obtain the corresponding vector of coefficient $\{c\}_n$ by solving $[Q(\omega_n)]\{c\}_n = 0$. $\{c\}_n$ can also be estimated as the eigenvector corresponding to the minimum eigenvalue of $[Q(\omega_n)]$ [35]. By substituting $\{c\}_n$ in equation (18), the mode shape $\{z\}_n$ corresponding to natural frequency ω_n is obtained. Although this procedure for finding natural frequencies and mode shapes seems straightforward, it cannot be effectively applied to all situations due to the possibility of numerical ill-conditioning, especially when dimensions of $[Q(\omega)]$ becomes large, e.g., in multi-stepped rotor modeling. This deficiency is highlighted by using an example in the next section.

An alternative method for finding natural frequencies is proposed in this paper. Since $|Q(\omega)| = \prod_{r=1}^{N} \bar{\lambda}_r \, , N = 1,2, \dots, 40$, there is a possibility of $|Q(\omega)|$ to become near-zero even at frequencies that are not the natural frequencies; this could be the result of the multiplication of several small eigenvalues $\bar{\lambda}_r$ of $[Q(\omega)]$ which makes finding the natural frequencies by employing $|Q(\omega)| = 0$ difficult.

Based on this fact that at natural frequencies, there is always one zero eigenvalue for $[Q(\omega)]$, the natural frequencies can also be found by using the condition number of $[Q(\omega)]$- i.e. $\bar{\kappa}(Q)$- as,

$$h(\omega) = \frac{1}{\bar{\kappa}(Q)} = \frac{|\bar{\lambda}_{min}|}{|\bar{\lambda}_{max}|} = 0 \qquad (21)$$

The following section shows that equation (21) is much more effective than equation (20) in finding natural frequencies.

The other application of equation (19) is identifying system parameters when a few natural frequencies are known. [36] and [37] used the characteristic equation and identified the unknown parameters of mechanical systems. The use of characteristic equation can be summarized as,

$$min \|\mathcal{F}(p_1, p_2, \dots, p_z)\| \quad \text{subject to} \quad p_1, p_2, \dots, p_z > 0 \qquad (22)$$

where p_1, p_2, …, p_z are system parameters and $\mathcal{F}$ is defined as,

$$\mathcal{F}(p_1, p_2, \dots, p_z) = [q(\omega_1) \quad q(\omega_2) \quad \dots \quad q(\omega_l)]^T \qquad (23)$$

The use of equation (21) instead of equation (20) in the objective function of equation (23) is proposed in this paper which results in $\mathcal{F}$ to be defined as,

$$\mathcal{F}(p_1, p_2, \dots, p_z) = [h(\omega_1) \quad h(\omega_2) \quad \dots \quad h(\omega_l)]^T \qquad (24)$$

Equation (24) can be solved using numerical optimization approaches, and the unknown system parameters can be identified. A numerical example is considered

in the next section to show the effectiveness of equation (21) over equation (20) in finding natural frequencies.

4. Representative example

A numerical example consisting of a multi-stepped rotor is considered in this section to demonstrate the applicability of the theoretical modeling approach developed in previous sections. The rotor, made of steel ($E = 210$ GPa, $\rho = 7800$ kg/m^3), has 11 sections and is supported at the two ends by lateral and torsional spring elements, i.e. k_w and k_θ representing the effect of bearings. A schematic of the rotor is shown in Fig. 5, and the dimensions of its different sections are tabulated in Table 3. The cross-section is solid in all sections.

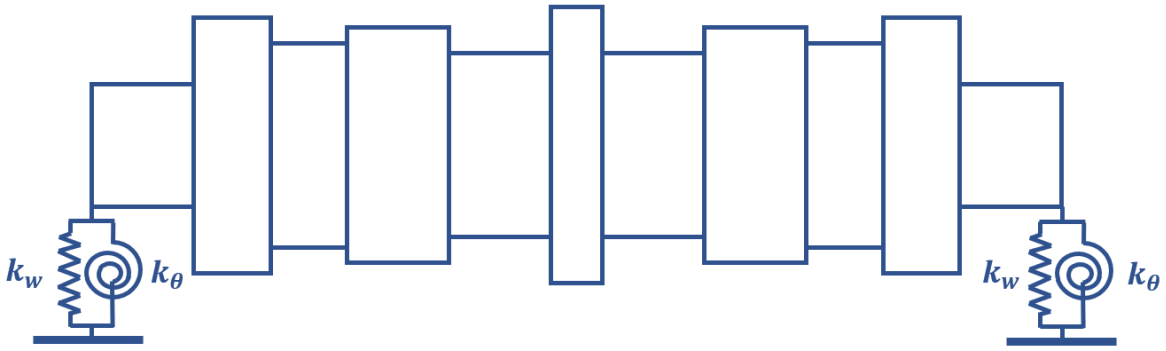

Figure 5- schematic of the multi-stepped rotor

Table 3- diameter and length of different sections of the rotor (cm)

Sec. No.	1	2	3	4	5	6	7	8	9	10	11

D	24	50	40	46	36	54	36	46	40	50	24
L	20	15	15	20	20	10	20	20	15	15	20

The modeling approach described in the previous section is used to analyze the free vibration response of a multi-stepped rotor. The boundary conditions at the two endpoints of the rotor are defined as,

$$k_\theta \psi_1(x,t) - (EI)_1 \frac{\partial \psi_1(x,t)}{\partial x} = k_w w_1(x,t) - (\kappa GA)_1 \left(\frac{\partial w_1(x,t)}{\partial x} - \psi_1(x,t)\right) = 0, \quad at \quad x = 0 \qquad (25)$$

$$k_\theta \psi_{11}(x,t) + (EI)_{11} \frac{\partial \psi_{11}(x,t)}{\partial x} = k_w w_{11}(x,t) + (\kappa GA)_{11} \left(\frac{\partial w_{11}(x,t)}{\partial x} - \psi_{11}(x,t)\right) = 0, \quad at \quad x = L \qquad (26)$$

Natural frequencies are obtained using the analytical method introduced in the previous section. Fig. 6 shows the results of using equations (20) and (21) in finding natural frequencies for different values of bearing stiffness coefficients,

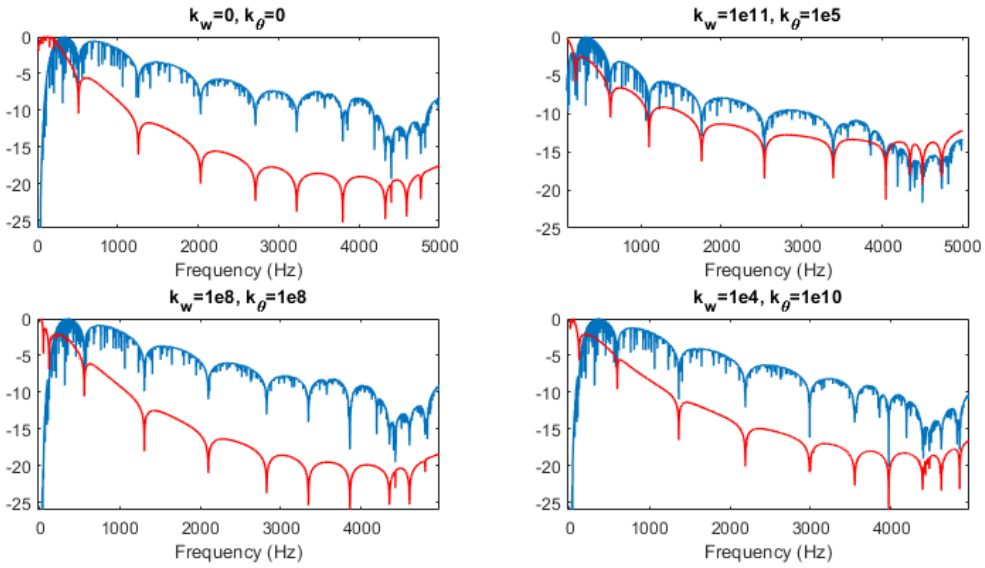

Figure 6- Variation of $log\left(|q|/max(q)\right)$ (blue) and $log\left(|h|/max(h)\right)$ (red) by frequency ω

Fig. 6 shows that in contrast to equation (20), equation (21) can be effectively used to extract the natural frequencies. In Table (4), the natural frequencies obtained by using $h(\omega)$ in Fig. 6 are compared with counterparts from a finite element model in *ANSYS* using Timoshenko beam elements *Beam181*. 1 cm element sizes were used in the F.E. model.

Table 4-Comparing natural frequencies for multi-stepped rotor (Hz)

	ω_1	ω_2	ω_3	ω_4	ω_5	ω_6	ω_7	ω_8	ω_9
$k_w = 0\ (\frac{\mathrm{N}}{\mathrm{m}})\ ,\ k_\theta = 0\ (\frac{\mathrm{Nm}}{\mathrm{rad}})$									
FEM	512.9	1251.7	2017.4	2694.5	3194.1	3766.2	4281.7	4344.6	4546.5
Present	513.7	1257.3	2031	2713	3225.3	3797.7	4326.5	4399.8	4591.5
Error (%)	0.2	0.4	0.7	0.7	0.9	0.8	1.0	1.3	1.0
$k_w = 1\times10^{11}\ (\frac{\mathrm{N}}{\mathrm{m}})\ ,\ k_\theta = 1\times10^{5}\ (\frac{\mathrm{Nm}}{\mathrm{rad}})$									
FEM	190.6	617.9	1095.9	1744.9	2516.1	3369.0	4001.2	4293.2	4451.1
Present	190.9	621	1102.3	1755.2	2536.4	3391.2	4044.1	4346.9	4502.2
Error (%)	0.2	0.5	0.6	0.8	0.7	0.7	1.1	1.3	1.1
$k_w = 1\times10^{8}\ (\frac{\mathrm{N}}{\mathrm{m}})\ ,\ k_\theta = 1\times10^{8}\ (\frac{\mathrm{Nm}}{\mathrm{rad}})$									
FEM	50.3	120.3	557.5	1298.4	2084.7	2804.7	3309.0	3823.5	4303.1
Present	50.4	120.2	558.4	1304.1	2098.8	2825.0	3344.3	3860.1	4350.7
Error (%)	0.2	0.0	0.2	0.4	0.7	0.7	1.1	0.9	1.1
$k_w = 1\times10^{4}\ (\frac{\mathrm{N}}{\mathrm{m}}),\ k_\theta = 1\times10^{10}\ (\frac{\mathrm{Nm}}{\mathrm{rad}})$									
FEM	123.1	596.5	1355.9	2173.5	2967.9	3507.4	3925.1	4339.6	4421.1

Present	123.2	598.7	1362.1	2189.8	2990	3548.2	3972.0	4393.1	4476.6
Error (%)	0.1	0.4	0.4	0.7	0.7	1.2	1.2	1.2	1.3

Results presented in Table (4) show the analytical method's efficiency introduced in previous sections for modeling multi-stepped rotors. The minor discrepancies between F.E. and the method used in this paper could result from discretization in FEM since all errors are positive, which shows that the F.E. model is stiffer than the analytical model. The following section considers identifying the rotor-armature parameters by using experimental results.

5. Rotor-armature model characterization

In this section, the model developed for rotor-armature in previous sections is characterized, and its unknown parameters are identified using experimentally measured results. As explained in previous sections, there are two types of parameters to be identified for this structure: material properties of the armature and parameters of the contact interface between shaft and armature. These parameters are identified by minimizing the differences between experimental and numerical natural frequencies. Numerical natural frequencies are obtained using the modeling approach described in previous sections. Minimization is performed using *MATLAB Optimization Toolbox.* The identified parameters and the comparison between numerical and experimental results are shown in Tables 5 and 6, respectively.

Table 5- Identified parameters for the rotor-armature model

E_a (Pa)	ρ_a $(\frac{\text{kg}}{\text{m}^3})$	k_w $(\frac{\text{N}}{\text{m}})$	k_θ $(\frac{\text{Nm}}{\text{rad}})$
76943391600	6035	413397935	311125997

The identified material properties for armature are reasonable. As stated before, the armature is made of copper coils inserted into armature slots. Therefore, its density and modulus of elasticity should be less than a solid object made of copper. The material properties of copper are $E_c = 130\ GPa$ and $\rho_c = 8960\ kg/m^3$. To further investigate the accuracy of the model identified for the rotor, an F.E. model is created in *ANSYS* using Timoshenko beam elements *Beam181* for representing shaft and armature and spring elements COMBIN14 for considering the contact effects between shaft and armature. Table 6 shows the natural frequencies obtained from *ANSYS* and their difference from experimental natural frequencies. Table 6 shows a higher discrepancy for the results obtained from ANSYS compared to the modeling method used in this paper with respect to experimental results, which is due to discretization error.

Table 6- Comparing numerical and experimental natural frequencies (Hz)

	ω_1	ω_2	ω_3	ω_4	ω_5
Exp.	103.1	173.4	232.8	389.1	610.9
Num.	111.4	168.5	215.6	387.6	605.2
Error (%)	8.1	-2.8	-7.4	-0.4	-0.9
ANSYS	112.1	166.5	218.2	385.3	603.9
Error (%)	8.7	-3.9	-6.2	-0.9	-1.1

Considering the structural complexities of rotor-armature and simplifications made in modeling- for example, a uniform distribution for contact interface stiffness is assumed in the modeling while the actual stiffness distribution is not constant- the accuracy of the results in Table 6 is acceptable. In Figure (6), $q(\omega)$ and a spline fitted on $h(\omega)$ for the identified rotor-armature model are shown to emphasize the effectiveness of using equation (21) instead of equation (20).

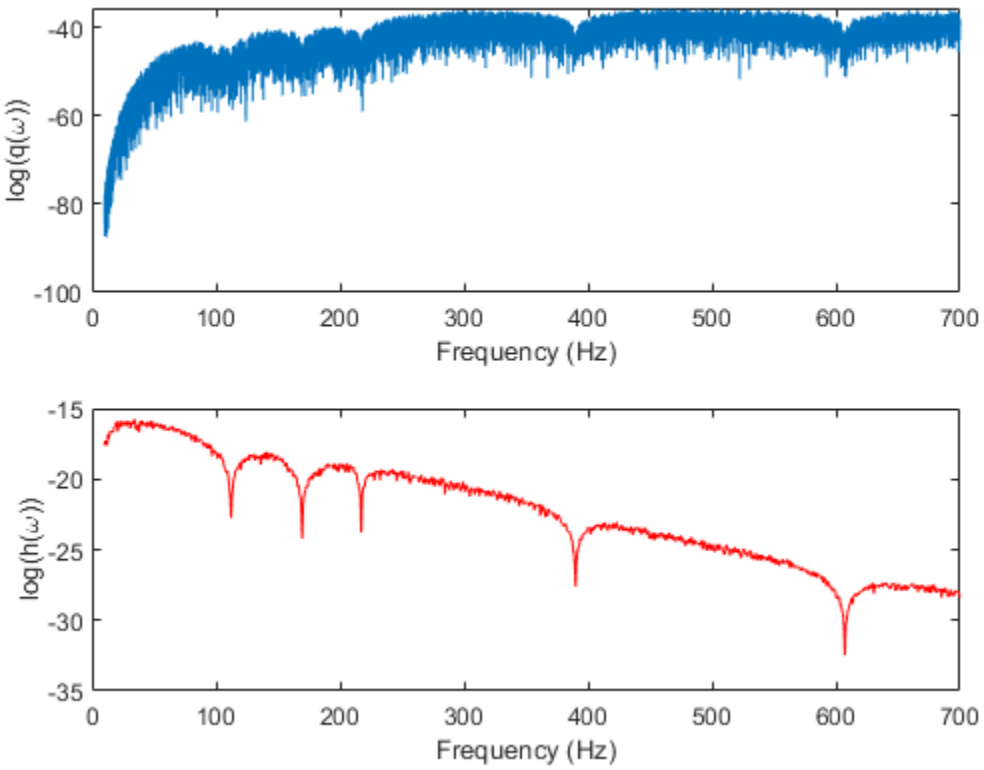

Figure 7 - comparing $q(\omega)$ and $h(\omega)$ for the identified rotor-armature model

The mode shapes of the identified rotor-armature model are shown in Figure (8). The mode shapes reveal potential interactions between rotor and armature, leading to nonlinear behaviors in the contact interface such as micro/macro slip and micro-vibro-impacts. Nonlinearity in the contact interface and its effect on the overall dynamic response of the rotor-armature structure could be the subject of future

research in this area. Also, the verified dynamic model obtained for rotor-armature structure can be used for fault diagnoses purposes. For instance, the effect of loosening in the joints connecting shaft to armature on the critical speeds can be studied by using this model.

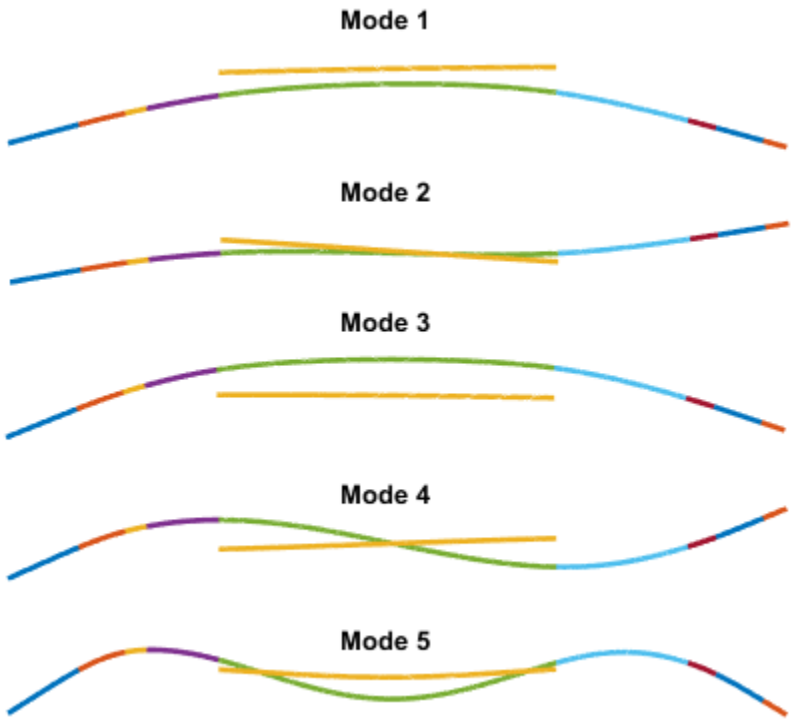

Figure 8- The mode shapes from identified rotor-armature model

6. Discussion and future work

This study presents a new field problem for applying a mathematical modeling and experimental updating strategy. The ongoing research includes investigating a wide range of experimental modal tests conducted on the rotor-armature structure while located at several angular positions, both in free-free and on-bearing boundary conditions. These tests were performed to identify if faults such as crack or looseness exist in the rotor assembly suspected due to abnormal behaviors of the turbine during

operation. Figure 9 shows an example of 1.5% variations of the first measured natural frequency and the corresponding FRFs obtained in the free-free conditions.

The modeling and verification strategies presented in this work will be employed to investigate the existence and location of a possible crack/looseness using the complete set of experimental results. A reduction in the identified may simply determine fault location k_θ and k_w parameters along the rotor in each test. Correlations between the identified parameters in tests at different angular positions will help a solid conclusion on fault diagnosis on the rotating structure.

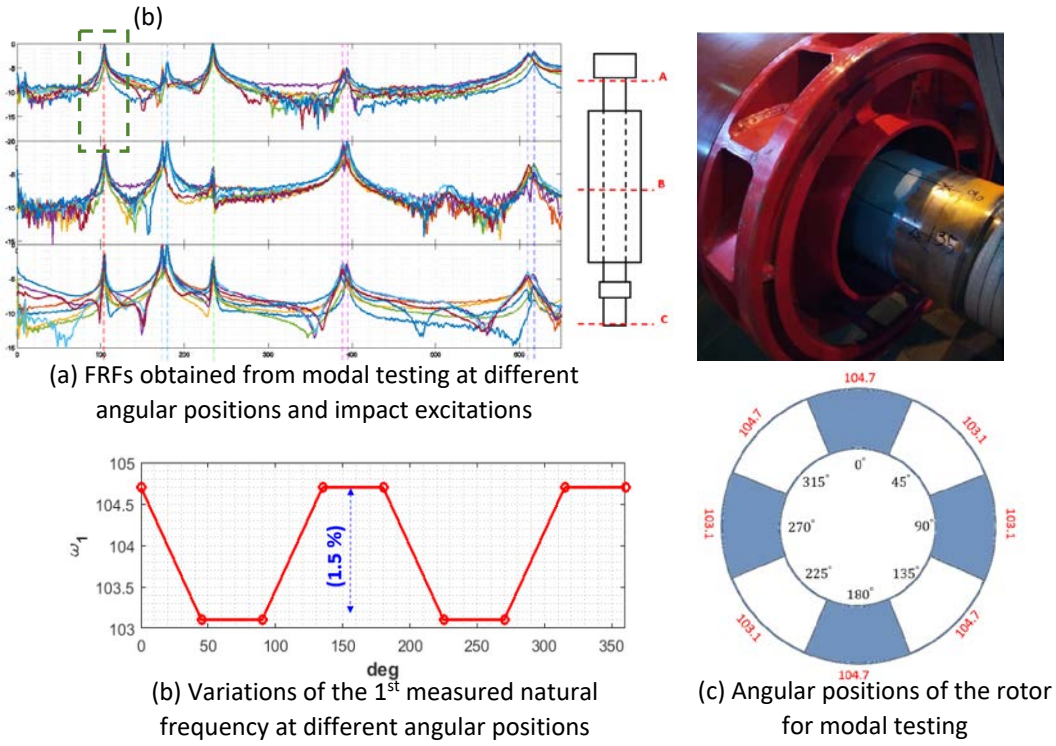

(a) FRFs obtained from modal testing at different angular positions and impact excitations

(b) Variations of the 1st measured natural frequency at different angular positions

(c) Angular positions of the rotor for modal testing

Figure 9: Future trend of the research for employing the verified dynamic model of the rotor-armature structure

7. Conclusion

A verified model for a rotor-armature structure was discussed in this paper. Timoshenko beam theory was used in analytical modeling of the rotor, which is a multi-stepped beam structure. The effects of the contact interface between rotor and armature were included in the analytical model employing uniform distributed linear spring elements. The accuracy of analytical modeling and the proposed approach for obtaining natural frequencies was verified by comparing the natural frequencies of a multi-stepped rotor with the results from an F.E. counterpart. Test results were used to identify unknown parameters in the rotor-armature structural model. The identified model generates promising results and can serve as a base linear model in nonlinear rotor-armature interaction and fault diagnostic analyses. The novelty of this paper is twofold as in following,

- A method was proposed based on the condition number of the coefficient matrix in analytical modelling for finding natural frequencies.
- Mathematical modelling and experimental updating strategies were used in a new field problem in rotor dynamics.

The main findings of this research are,

- The frictional contact interfaces in rotating machinery significantly affect the dynamic response, introducing difficulties in numerical modelling. They need to be considered carefully in dynamic modelling.
- A uniform distribution of spring elements can be used to consider the linear effects of frictional contact interfaces in rotor dynamics.
- A proper approach needs to be used for calculating natural frequencies when analytical modelling is adopted.

8. Appendix

All arrays of $[F]_{20\times20}$ are zero unless for the followings,

$$F(9,9)=k_w,\ F(9,19)=-k_w,\ F(19,9)=-k_w,\ F(19,19)=k_w \tag{A1}$$

$$F(10,10)=k_t,\ F(10,20)=-k_t,\ F(20,10)=-k_t,\ F(20,20)=k_t \tag{A2}$$

Substituting $\{V(x,t)\}=\{Y(x)\}e^{j\omega t}$ into equations (7-13) results in the following boundary conditions,

$$(EI)_1\Phi_1'(x)=(\kappa GA)_1(\mathrm{Y}_1'(x)-\Phi_1(x))=0,\quad at\quad x=0 \tag{A3}$$

$$(EI)_9\Phi_9'(x)=(\kappa GA)_9(\mathrm{Y}_9'(x)-\Phi_9(x))=0,\quad at\quad x=L \tag{A4}$$

$$(EI)_{10}\Phi_{10}'(x)=(\kappa GA)_{10}(\mathrm{Y}_{10}'(x)-\Phi_{10}(x))=0,\quad at\quad x=L_1 \tag{A5}$$

$$(EI)_{10}\Phi_{10}'(x)=(\kappa GA)_{10}(\mathrm{Y}_{10}'(x)-\Phi_{10}(x))=0,\quad at\quad x=L_2 \tag{A6}$$

$$Y_s(x_s)=Y_{s+1}(x_s),\ \Phi_s(x_s)=\Phi_{s+1}(x_s),\qquad x_s=\textstyle\sum_{r=1}^{s}L_r\,,\quad s=\ 1,2,\dots,8 \tag{A7}$$

$$(EI)_s\Phi_s'(x)=(EI)_{s+1}\Phi_{s+1}'(x),\ x_s=\textstyle\sum_{r=1}^{s}L_r\,,\quad s=\ 1,2,\dots,8 \tag{A8}$$

$$(\kappa GA)_s\left(\mathrm{Y}_s'(x)-\Phi_s(x_s)\right)=(\kappa GA)_{s+1}\left(\mathrm{Y}_{s+1}'(x)-\Phi_{s+1}(x_s)\right),,\ x_s=\textstyle\sum_{r=1}^{s}L_r\,,\quad s=\ 1,2,\dots,8 \tag{A9}$$

where $(\quad)'=\frac{d(\quad)}{dx}$.

9. Acknowledgments

The authors are grateful to Abbas Hassani from Shazand Thermal Power Plant for his cooperation in performing the experimental vibration tests on the rotor-armature structure.

10. References

[1] Z. Racic, B. Sun, N. Boyle, Diagnosis and solution of the exciter rotor vibration problem, in: International Symposium on Transport Phenomena and Dynamics of Rotating machinery (ISROMAC), 1998, pp. 394

[2] K. Xia, Y. Sun, D. Hong, J. Guo, X. Kang, Effects of contact interfaces on rotor dynamic characteristics of heavy-duty gas turbine generator set, in: IEEE International Conference on Mechatronics and Automation, IEEE, Harbin, China, 2016, pp. 714-719.
[3] Q. Yuan, R. Gao, Z. Feng, J. Wang, Analysis of dynamic characteristics of gas turbine rotor considering contact effects and pre-tightening force, in: ASME Turbo Expo 2008: Power for Land, Sea, and Air, Berlin, Germany, 2008, pp. 983-988.
[4] L. Mingjian, G. Haipeng, Y. Baisong, Y. Lie, Finite element method for disc-rotor dynamic characteristics analysis of gas turbine rotor considering contact effects and rod preload, in: IEEE International Conference on Mechatronics and Automation, IEEE, Xi'an, China, 2010, pp. 1179-1183.
[5] Z. Yanchun, D. Zhaogang, S. Liming, L. Shaoquan, Determination of contact stiffness of rod-fastened rotors based on modal test and finite element analysis, Journal of Engineering for Gas Turbines and Power, 132 (2010).
[6] E.J. Gunter, Influence of flexibly mounted rolling element bearings on rotor response: Part I—Linear analysis, Journal of Lubrication Technology, 92 (1970) 59-69.
[7] R. Rzadkowski, A. Maurin, Multistage coupling of eight mistuned bladed discs on a solid shaft of the steam turbine, Forced Vibration Analysis, J Vib Eng Technol, 2 (2014) 495-508.
[8] S. Bograd, P. Reuss, A. Schmidt, L. Gaul, M. Mayer, Modeling the dynamics of mechanical joints, Mechanical Systems and Signal Processing, 25 (2011) 2801-2826.
[9] F. Pourahmadian, H. Ahmadian, H. Jalali, Modeling and identification of frictional forces at a contact interface experiencing micro-vibro-impacts, Journal of Sound and Vibration, 331 (2012) 2874-2886.
[10] J.L. do Vale, C.H. da Silva, Kinetic friction coefficient modeling and uncertainty measurement evaluation for a journal bearing test apparatus, Measurement, 154 (2020) 107470.
[11] H. Jalali, H.H. Khodaparast, H. Madinei, M.I. Friswell, Stochastic modelling and updating of a joint contact interface, Mechanical Systems and Signal Processing, 129 (2019) 645-658.
[12] A.D. Dimarogonas, S.A. Paipetis, T.G. Chondros, Analytical methods in rotor dynamics, Springer, 2013.
[13] A. Sinha, Reduced-order model of a bladed rotor with geometric mistuning, Journal of Turbomachinery, 131 (2009).
[14] S. Wang, Y. Wang, Y. Zi, B. Li, Z. He, Reduced-order modeling for rotating rotor-bearing systems with cracked impellers using three-dimensional finite element models, Journal of Sound and Vibration, 355 (2015) 305-321.
[15] D.J. Segalman, T. Paez, D. Smallwood, A. Sumali, A. Urbina, Status and integrated road-map for joints modeling research, Sandia National Laboratories, Albuquerque, NM, (2003).
[16] A. Sagheer, Rotor casing contact phenomenon in rotor dynamics — Literature survey, Journal of Vibration and Control, 16 (2010) 1369-1377.
[17] G. Jacquet-Richardet, M. Torkhani, P. Cartraud, F. Thouverez, T. Nouri Baranger, M. Herran, C. Gibert, S. Baguet, P. Almeida, L. Peletan, Rotor to stator contacts in turbomachines. Review and application, Mechanical Systems and Signal Processing, 40 (2013) 401-420.
[18] H. Ma, X. Tai, Q. Han, Z. Wu, D. Wang, B. Wen, A revised model for rubbing between rotating blade and elastic casing, Journal of Sound and Vibration, 337 (2015) 301-320.
[19] H. Ma, D. Wang, X. Tai, B. Wen, Vibration response analysis of blade-disk dovetail structure under blade tip rubbing condition, Journal of Vibration and Control, 23 (2015) 252-271.
[20] Y. Li, Z. Luo, Z. Liu, X. Hou, Nonlinear dynamic behaviors of a bolted joint rotor system supported by ball bearings, Archive of Applied Mechanics, 89 (2019) 2381-2395.
[21] P. Yu, L. Li, G. Chen, M. Yang, Dynamic modelling and vibration characteristics analysis for the bolted joint with spigot in the rotor system, Applied Mathematical Modelling, 94 (2021) 306-331.
[22] Y. Li, Z. Luo, B. Shi, J. Liu, Influence of contact interface friction of bolted disk joint on motion stability of rotor-bearing system, Archive of Applied Mechanics, (2021).

[23] Z. Qin, Q. Han, F. Chu, Bolt loosening at rotating joint interface and its influence on rotor dynamics, Engineering Failure Analysis, 59 (2016) 456-466.
[24] L. Shuguo, M. Yanhong, Z. Dayi, H. Jie, Studies on dynamic characteristics of the joint in the aero-engine rotor system, Mechanical Systems and Signal Processing, 29 (2012) 120-136.
[25] M. Zhuo, L.H. Yang, L. Yu, Contact stiffness calculation and effects on rotordynamic of rod fastened rotor, in: ASME 2016 International Mechanical Engineering Congress and Exposition, 2016.
[26] S. Edwards, A. Lees, M. Friswell, The influence of torsion on rotor/stator contact in rotating machinery, Journal of Sound and Vibration, 225 (1999) 767-778.
[27] J. Oh, 3D solid finite element rotordynamics: Parametric stability analysis and contact modeling, in: Mechanical Engineering, Texas A&M University, 2020.
[28] J. Oh, B.J. Kim, A. Palazzolo, Three-dimensional solid finite element contact model for rotordynamic analysis: Experiment and simulation, Journal of Vibration and Acoustics, 143 (2020).
[29] A.M. Rimpel, A simple contact model for simulating tie bolt rotor butt joints with and without pilot fits, in: ASME Turbo Expo 2018: Turbomachinery Technical Conference and Exposition, 2018.
[30] A.M. Rimpel, M. Leopard, Simple contact stiffness model validation for tie bolt rotor design with butt joints and pilot fits, Journal of Engineering for Gas Turbines and Power, 142 (2019).
[31] D.J. Ewins, Modal testing: Theory, practice and application, 2nd edition ed., Wiley, 1999.
[32] S.-W. Hong, J.-H. Park, Dynamic analysis of multi-stepped, distributed parameter rotor-bearing systems, Journal of Sound and Vibration, 227 (1999) 769-785.
[33] G.R. Cowper, The shear coefficient in Timoshenko's beam theory, Journal of Applied Mechanics, 33 (1966) 335-340.
[34] S.S. Rao, Vibration of continuous systems, Wiley Online Library, 2007.
[35] R.T. Haftka, Z. Gürdal, Elements of structural optimization, Springer Science & Business Media, 2012.
[36] H. Ahmadian, J.E. Mottershead, M.I. Friswell, Boundary condition identification by solving characteristic equations, Journal of Sound and Vibration, 247 (2001) 755-763.
[37] H. Jalali, Linear contact interface parameter identification using dynamic characteristic equation, Mechanical Systems and Signal Processing, 66 (2016) 111-119.